American Mineralogist, Volume 91, pages 794–801, 2006

Single-crystal diffraction and transmission electron microscopy studies of "silicified" pyrochlore from Narssârssuk, Julianehaab district, Greenland

PAOLA BONAZZI,[1,*] LUCA BINDI,[1] MATTEO ZOPPI,[1] GIAN CARLO CAPITANI,[2] AND FILIPPO OLMI[3]

[1]Dipartimento di Scienze della Terra, Università di Firenze, Via La Pira 4, I-50121, Firenze, Italy
[2]Dipartimento di Scienze della Terra, Università di Siena, Via Laterina 8, I-53100, Siena, Italy
[3]CNR, Istituto di Geoscienze e Georisorse–sezione di Firenze, Via La Pira 4, I-50121, Firenze, Italy

ABSTRACT

Pyrochlore-group minerals that exhibit high Si contents are fairly common in geochemically evolved parageneses. However, the role of Si in the structure of these minerals is unclear. Different explanations have been invoked to clarify the way in which Si is incorporated in natural pyrochlores. These include the presence of impurities, the presence of Si in an amorphous or dispersed state, and its presence as an essential part of the structure.

This paper reports an integrated XREF, SEM, EMPA, and TEM study on pyrochlore samples with high SiO_2 content (up to 11.51 wt%) from Narssârssuk, Julianehaab district (Greenland). TEM observations reveal that Si-poor areas have strong and sharp diffraction peaks, whereas the Si-rich areas showed weaker spots with the diffuse diffraction halo typical of a metamict material. No evidence of crystalline phases other than pyrochlore was observed. Two single crystals having the unit-cell parameter a = 10.4200(7) and 10.3738(7) Å, respectively, were analyzed by X-ray diffraction and the structure was refined to R_{obs} = 2.62 and 4.35%. On the basis of both the refined site scattering and the octahedral bond distance and the results of the TEM investigation, only a fraction (~30–50%) of the Si detected by EMPA is incorporated in the structure. A comparison with structural data of Si-free pyrochlores reported in the literature supports this assumption and allows a linear multiple regression to model the effect of the substitution of (Nb,Ta) by Ti and Si. The remaining 50–70% of the total silicon detected is incorporated in the radiation-damaged portions of pyrochlore.

Keywords: Pyrochlore, electron microscopy, crystal structure, XRD data, analysis, chemical (mineral)

INTRODUCTION

Pyrochlore-group minerals, space group $Fd\bar{3}m$, have the general formula $A_{2-m}B_2X_6Y_{1-n}\cdot pH_2O$, where m = 0.0–1.7, n = 0.0–1.0 and p = 0.0–2.5 (Lumpkin et al. 1986). At n = 0, A is an eightfold-coordinated cation (mostly Ca and Na, with K, Sr, Ba, Sn^{2+}, Pb^{2+}, REE^{3+}, Y, Sb^{3+}, Bi^{3+}, U^{4+}, and Th^{4+} occurring less commonly or in lesser amounts) whereas B is an octahedrally coordinated cation, namely Nb, Ta, and Ti^{4+} (or Sb^{5+} in the stibiconite mineral group) with minor quantities of Fe^{3+}, Sn^{4+}, and W^{6+}. The X position is mostly occupied by O^{2-} or, to a lesser extent, OH^- (Ercit et al. 1993, 1994; Nasraoui and Waerenborgh 2001), whereas Y may be O^{2-}, OH^-, or F^-. Pyatenko (1959) was the first to recognize that the pyrochlore structure is a derivative of the fluorite structure. The pyrochlore structure can be derived from the fluorite structure by removing 1/8 of the anions in an ordered fashion such that one half of the cubic polyhedra lack two opposed vertices (Chakoumakos 1984). In this type of structure, named *normal* pyrochlore, both the A and Y site can be partially vacant (m < 2, n < 1). Alternatively, the structure is referred to *inverse* pyrochlore when the Y site is occupied by large ionic radius cations (i.e., K, Tl^+, Rb, Cs) with the A position remaining vacant. A mixed *inverse-normal* pyrochlore structure has been described for cesstibtantite and kalipyrochlore (Ercit et al. 1993, 1994).

Minerals of the pyrochlore group typically occur as accessory minerals in granitic pegmatites, nepheline-syenite pegmatites, and carbonatites. They are stable under a wide range of *P-T* conditions ranging from igneous to near-surface. Although most natural pyrochlore-group minerals satisfy the definition of pyrochlore sensu stricto, microlite, or betafite, several other species have been defined based on the dominance of an A cation other than Ca or Na (for nomenclature rules see Hogarth 1977). Furthermore, a wide range of different elements can be incorporated as minor components. Thus, several authors commonly also include Mg, Mn^{2+}, or Fe^{2+} and Al, Si, or Fe^{3+} in the chemical formula as A and B cations, respectively. In particular, the presence of a high Si content raises questions about the role of Si in the structure of pyrochlore minerals. Although $Si(OH)_6$ octahedra are present in the structure of thaumasite at room pressure (Edge and Taylor 1971), sixfold-coordinated Si is usually restricted to high-pressure minerals (Finger and Hazen 1991). Accordingly, $Sc_2Si_2O_7$ and $In_2Si_2O_7$ pyrochlore-type compounds with Si located in the octahedral B site have been synthesized at T = 1000 °C and P = 12 GPa (Reid et al. 1977). The isomorphous germanates ($A_2Ge_2O_7$, with A = Sc, Y, In, Gd-Lu, Tl), which are synthesized commonly at lower pressure compared to the corresponding silicates, also require a high pressure for their

* E-mail: pbcry@geo.unifi.it

synthesis (P = 6.5 GPa) (Shannon and Sleight 1968).

On the other hand, a crystalline antimony-silicate with pyrochlore-type structure was obtained by acidic hydrolysis of Sb^{5+} and Si^{4+} (pH < 1) at a room pressure and temperature of 60 °C (Möller et al. 2001a). As the unit-cell parameter of such a compound [a = 10.391(2) Å] is close to that of Si-free hydrous antimony pentoxide (10.38 Å), and assuming that cation substitutions at the A site affect the unit-cell parameter less than those at the B site, Möller et al. (2001b) suggested that Si could enter the A site. This explanation seems implausible, and Möller et al. did not rule out the presence of impurity phases, such as amorphous SiO_2.

The presence of Si in the structure of pyrochlore group minerals has been long debated but has not been resolved. Despite the absence of tetrahedral sites suitable for Si incorporation in the pyrochlore structure, and the unlikely octahedral coordination for Si under physical conditions in which pyrochlore forms, the hypothesis that Si is hosted within the structure is, in large part, due to the wide-spread reports of Si-rich pyrochlores. Hogarth (1977, 1989) suggested the high Si content could be due to the presence of impurities while Voloshin et al. (1989) proposed that it results from the possible presence of Si "in an amorphous or dispersed state."

To understand the way in which Si is incorporated into the structure of pyrochlore, we carried out an integrated study of samples with high silica content based on X-ray refinement (XREF), scanning electron microprobe (SEM), electron microprobe analyses (EMPA), and transmission electron microscopy (TEM).

Occurrence of "silicified" pyrochlores

Si-rich pyrochlores were first reported by Flink (1898, 1901) from nepheline syenites at Narssârssuk, Julianehaab district (Greenland). Two pyrochlore-type minerals containing SiO_2 of 10.86 and 11.48 wt% were named "chalcolamprite" and "endeiolite," respectively. They were similar in composition, but the first mineral had higher fluorine content. According to Bøggild (1953) "chalcolamprite" and "endeiolite" were found frequently intergrown with needles of aegirine. Hogarth (1977) suggested that such a high content of SiO_2 could be due to interference from the spatially associated aegirine, so that both minerals were discredited.

Pyrochlore with SiO_2 contents ranging from 7.37 to 10.12 wt% and accompanied by high analytical deficits has been reported as accessory minerals in the Cínovec (Zinnwald) granite cupola, Czech Republic (Johan and Johan 1994). This pyrochlore is enriched in uranium, and shows an elevated vacancy at the A site. Based on the negative correlation of Si with Σ(Nb, Ta, W, Ti, Sn, Zr), Johan and Johan (1994) hypothesized incorporation of Si at the B site.

An elevated SiO_2 content (up to 9.49 wt%) in U-rich, Pb-rich pyrochlore from the Prašivá granitic pegmatites (Slovakia) was reported by Uher et al. (1998). They discussed possible mechanisms to compensate for the charge deficiency caused by the presence of Si (up to 0.70 apfu) on the B site. Contrary to this view, Hogarth et al. (2000) suggested that the presence of Si (ranging from 3.03 to 3.84 wt% SiO_2) in the metamict, zoned uranpyrochlore from McCloskey's Field (Quebec) was due to impurities of sub-micrometer silicate phases rather than to a Si ↔ Nb substitution.

Exceptionally high contents of Si (up to 16.8 wt% SiO_2) in pyrochlore-group minerals from metasomatic rocks of the Lovozero alkaline complex, Russia (Chakhmouradian and Mitchell 2002) were associated with highest A-cation deficiency and H_2O contents. By comparing the chemical data of these samples with those from other occurrences, Chakhmouradian and Mitchell (2002) found a negative correlation between the Si and (Nb + Ti) contents. In their opinion, neither the presence of absorbed amorphous silica nor intergrowths with niobosilicates could explain this inverse correlation. They also noted that "the form of silica occurrence in pyrochlore remains enigmatic" and further studies are required. According to Chakhmouradian and Mitchell (2002) submicroscopic intergrowth of pyrochlores with komarovite might also explain the incorporation of Si in pyrochlore. Komarovite has a layered structure consisting of pyrochlore slabs connected by four-membered tetrahedral silicate rings (Krivokoneva et al. 1979; Balić-Žunić et al. 2002; Ferraris et al. 2004).

Materials studied and experimental techniques

Two minute fragments of the samples from Narssârssuk, Julianehaab district (Greenland) originally classified as "chalcolamprite" and "endeiolite" (Geologisk Museum of København, Denmark; catalog numbers 1982.396 and 1982.110, respectively) were selected for this study. "Chalcolamprite" forms minute octahedral crystals that overgrow aegirine crystals. Associated minerals include albite and minor epididymite and ancylite-(Ce). Octahedral crystals of "endeiolite" are also grown on aegirine and are associated with synchysite-(Ce) and elpidite.

For the structural study, two single crystals (labeled 396a and 110a, respectively) were selected and mounted on an automated single-crystal diffractometer equipped with a serial detector. In both cases, extended peak searches did not reveal any peaks other than those belonging to the pyrochlore structure. As a further test, both crystals were also mounted (exposure time of 120 s per frame; 40 mA × 40 kV) on a CCD-equipped diffractometer (Oxford Xcalibur 2), but no additional reflections were detected.

Unit-cell dimensions were determined by least-squares refinement of the setting angles of 25 high-θ equivalent reflections. Collected intensity data were reduced for Lorentz-polarization effects, and corrected for absorption using the semi-empirical method of North et al. (1968). A full-matrix least-squares refinement on F^2 was performed in the space group $Fd\bar{3}m$ (origin choice 2) using the program SHELXL-97 (Sheldrick 1997). Assuming a *normal* pyrochlore structure, the A cation was located at the Wyckoff position 16*d* (½, ½, ½), B cation at 16*c* (0, 0, 0), X at 48*f* (x, $^1/_8$ $^1/_8$), and Y at 8*b* ($^3/_8$, $^3/_8$, $^3/_8$). Site-scattering values were refined using neutral scattering curves for A (Ca vs. Na), B (Nb vs. Ti), X (O vs. □) and Y (F vs. □). Details of data collection and R indices are given in Table 1 whereas final atomic coordinates and anisotropic displacement parameters are reported in Table 2.

The crystals 396a and 110a and another portion (396b) of the original fragment 1982-396 were analyzed by means of a JEOL JXA-8600 electron microprobe. Major and minor elements were determined at 15 kV accelerating voltage and 20 nA beam current, with 30 s as counting time. For WDS analyses, the following lines were used: Si*K*α, Na*K*α, F*K*α, K*K*α, Ca*K*α, Ti*K*α, Mn*K*α, Fe*K*α, Sr*L*α, Nb*L*α, Sb*L*α, La*L*α, Ce*L*α, Pr*L*β, Nd*L*β, Ta*L*α, Pb*M*α, Th*M*α, and U*M*α. The estimated analytical precisions are: ±0.80 for Nb and Ca; ±0.50 for Na, Ti, and Si; ±0.30 for Ta, Fe, Sr, and K; ±0.20 for Mn, Pb, Sb, La, Ce, Pr, Nd, U, and Th (wt% ox.); ±0.30 F (wt% el.). The standards employed were: fluorite (F), kaersutite (Si, Ca, Fe), albite (Na), rutile (Ti), bustamite (Mn), sanidine (K), celestite (Sr), monazite (La, Ce, Pr, Nd), and pure elements (Nb, Sb, Ta, Pb, Th, U).

The remaining part (396c) of the original fragment of the sample 1982-396 was used for the TEM study. TEM mounts were prepared by ion milling of doubly polished petrographic thin sections, glued on 3 mm wide copper rings. To avoid electrostatic charging inside the microscope, the thin foils were carbon coated. TEM investigations were carried out with a JEOL JEM-2010 electron microscope (University of Siena) operating at 200 kV, with a theoretical point-to-point resolution of 1.94 Å, and equipped with a double tilt (±20°) specimen holder. An attached Oxford Link energy dispersive X-ray spectrometer (EDX) allowed semi-quantita-

tive analyses, using internal theoretical k-factors. Images were acquired on Fuji image plates (3000 × 3760 pixels, 14 bit gray levels), read and processed with the Science Lab 97 package of programs by Fuji Photo Films, Co. Ltd.

Results and discussion

The chemical compositions obtained from the single crystals studied and the analyses of the other portion (396b) of the original fragment 1982-396 are reported in Table 3. All Fe was assumed to be Fe^{3+} in B and all Mn to be Mn^{2+} in A. The chemical formulae were tentatively calculated on the basis of Σ (B cations) = 2 apfu, including or excluding Si (values with or without parentheses, respectively). Figure 1 shows a BSE image of part of the fragment 396b; a compositional heterogeneity is clearly evident, the darkest areas differing in their higher Si content and analytical deficit when compared to the lighter areas. According to Lumpkin and Ewing (1995), primary, transitional or secondary alteration of the pyrochlore-subgroup minerals from nepheline syenites lead to a general increase in A-site vacancies, mainly at the expense of Na^+. However, in the case of primary alteration, the loss of A cations is moderate and does not exceed 0.3–0.5 cations pfu, which are values lower than the A-site vacancies found in the samples studied here. Primary alteration can reasonably be ruled out also on the basis of the degree of hydration, which can be approximated by the analytical deficits (Table 3). In the samples studied by Lumpkin and Ewing (1995) the inferred water contents increase from primary (2–5 wt% H_2O) through transitional (4–12 wt% H_2O) to secondary alteration (8–14 wt% H_2O).

The content of large cations, such as Sr, Ba, and K, generally increases with the degree of alteration, reaching maximum values in the cases of kalipyrochlore and strontiopyrochlore from Lueshe (Zaire) and bariopyrochlore from Minas Gerais (Brazil), which are excellent examples of secondary alteration (Lumpkin and Ewing 1995). In the samples from Narssârssuk, the Na_2O content decreases with the increase of SiO_2. However, K_2O and SrO exhibit the opposite trend (Fig. 2) without reaching the high values typically associated with secondary alteration. Although the difference in rock type and climate makes it difficult to directly compare the type of alteration, it seems plausible that higher Si contents can be related to late-stage hydration by silica-rich fluids. However, this style of alteration does not appear to be strictly fracture-controlled (Fig. 1), as is the situation for secondary alteration (Lumpkin and Ewing 1992, 1995, 1996), which suggests a different, earlier-stage controlling mechanism of alteration.

Due to the unlikely incorporation of such a high Si content in the structure of pyrochlore and to the wide spread of the values observed (Table 3), TEM-EDX analyses (Table 4) and TEM imaging on the ultra-thin sample might be expected to show two distinct Si-bearing and Si-free phases, respectively.

Table 1. Crystal data and experimental details

	396a	110a
diffractometer	Bruker P4	Enraf-Nonius CAD4
cell parameter	a = 10.4200(7) (Å) V = 1131.37(8) (Å^3)	a = 10.3738(7) (Å) V = 1116.38(8) (Å^3)
crystal size (μm)	160 × 160 × 100	170 × 150 × 120
wavelength	Mo$K\alpha$ (26mA x 50kV)	Mo$K\alpha$ (26mA x 50kV)
theta-range (°)	1 – 35	1 – 35
range of hkl	$0 < h < 16$ $0 < k < 16$ $0 < l < 16$	$-16 < h < 16$ $0 < k < 16$ $0 < l < 16$
scan mode	ω	ω
scan width (°)	2.40	2.50
scan speed (°/min)	1.00/6.00	2.35
number of parameters	14	14
collected refl.	708	1341
independent refl.	147	146
refl. with $F_o > 4\sigma(F_o)$	128	99
R_{merge} (%)	6.59	8.95
R_{obs} (%)	2.62	4.35
R_{all} (%)	3.01	7.16
min ΔF peak (e$^-$/Å^3)	–0.40	–0.98
max ΔF peak (e$^-$/Å^3)	0.76	1.12

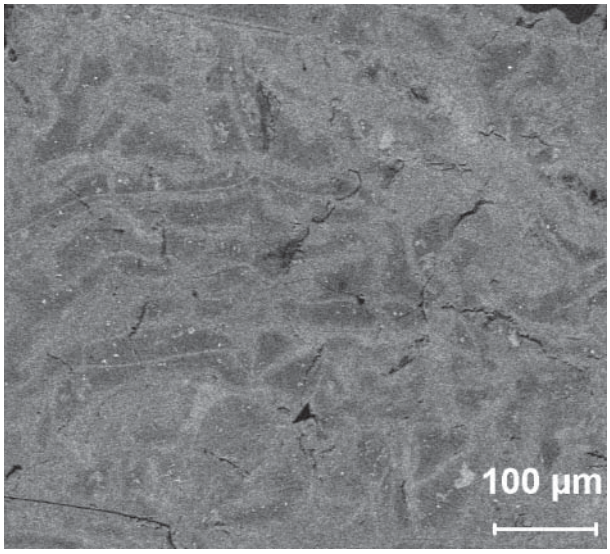

Figure 1. Backscattered-electron image (SEM) of a portion of the crystal used for the TEM investigation.

Table 2. Fractional atomic coordinates and anisotropic displacement parameters (Å^2) for the crystals examined

	*s.s.**	*x/a*	*y/b*	*z/c*	U_{11}	U_{22}	U_{33}	U_{12}	U_{13}	U_{23}	U_{eq}
396a											
A	14.9(1)	1/2	1/2	1/2	0.024(1)	U_{11}	U_{11}	0.0011(5)	U_{12}	U_{12}	0.024(1)
B	38.7(2)	0	0	0	0.0198(3)	U_{11}	U_{11}	–0.0018(1)	U_{12}	U_{12}	0.0198(3)
X	8.0(1)	0.3175(3)	1/8	1/8	0.027(2)	0.021(1)	U_{22}	0	0	0.008(1)	0.0228(8)
Y	8.4(1)	3/8	3/8	3/8	0.044(4)	U_{11}	U_{11}	0	0	0	0.044(4)
110a											
A	13.7(1)	1/2	1/2	1/2	0.026(2)	U_{11}	U_{11}	0.0053(9)	U_{12}	U_{12}	0.026(2)
B	36.3(2)	0	0	0	0.0225(5)	U_{11}	U_{11}	–0.0017(3)	U_{12}	U_{12}	0.0225(5)
X	8.0(1)	0.3173(6)	1/8	1/8	0.029(3)	0.028(2)	U_{22}	0	0	0.011(2)	0.028(1)
Y	8.4(1)	3/8	3/8	3/8	0.031(6)	U_{11}	U_{11}	0	0	0	0.031(6)

* Site scattering obtained by refining occupancy factor (see text).

TABLE 3. Electron microprobe analyses (oxides wt%) and atomic proportions for "silicified" pyrochlore crystals from Narssârssuk, Greenland

	396a		110a		396b	
	range	mean (no.* = 5)	range	mean (no.* = 7)	range	mean (no.* = 8)
Nb_2O_5	55.50–64.36	60.74	48.52–58.20	53.31	48.70–66.62	58.18
Ta_2O_5	1.28–1.82	1.50	2.52–3.11	2.83	–	–
TiO_2	2.63–4.25	3.30	2.89–3.66	3.36	2.62–4.16	3.68
Fe_2O_3	0.40–1.09	0.62	1.49–2.25	1.76	0.35–1.49	0.97
SiO_2	1.24–8.01	3.80	7.47–11.51	9.60	0.90–10.93	5.76
Na_2O	1.43–5.82	3.04	0.82–2.67	1.51	0.70–5.18	2.73
K_2O	0.06–0.42	0.28	0.39–0.81	0.60	0.12–0.52	0.29
CaO	9.53–12.64	10.91	9.94–11.71	10.97	8.70–12.01	10.22
SrO	1.16–2.90	2.01	1.54–2.98	2.12	1.10–3.77	2.49
MnO	0.60–0.85	0.68	0.67–0.86	0.76	0.47–1.20	0.92
PbO	0.62–0.90	0.72	0.41–0.57	0.47	0.29–0.78	0.53
La_2O_3	0.36–0.67	0.49	0.37–0.64	0.48	0.48–0.88	0.74
Ce_2O_3	0.02–1.84	1.22	1.32–1.75	1.59	1.05–2.23	1.93
Pr_2O_3	0.00–0.38	0.15	0.00–0.67	0.19	0.00–0.37	0.05
Nd_2O_3	0.29–0.41	0.29	0.00–0.51	0.32	0.00–0.49	0.36
UO_2	0.96–2.29	1.64	0.98–1.26	1.09	1.45–2.31	1.94
F	2.47–3.37	3.12	1.83–2.87	2.38	1.72–3.84	2.81
O=F	1.04–1.83	1.31	0.77–1.21	1.00	0.77–1.62	1.18
Total	91.66–95.77	93.20	89.38–96.34	92.32	84.72–98.17	92.40
Nb	1.75–1.82	1.78	1.62–1.71	1.68	1.70–1.82	1.77
	(1.38–1.70)	(1.59)	(1.16–1.34)	(1.26)	(1.19–1.75)	(1.48)
Ta	0.02–0.03	0.03	0.04–0.06	0.05	–	–
	(0.02–0.03)	(0.02)	(0.04)	(0.04)	–	–
Ti	0.13–0.19	0.16	0.15–0.20	0.18	0.16–0.23	0.19
	(0.11–0.18)	(0.14)	(0.11–0.15)	(0.13)	(0.11–0.18)	(0.16)
Fe	0.02–0.06	0.03	0.07–0.12	0.09	0.02–0.09	0.05
	(0.02–0.05)	(0.03)	(0.06–0.09)	(0.07)	(0.02–0.06)	(0.04)
Si	–	–	–	–	–	–
	(0.08–0.44)	(0.22)	(0.40–0.58)	(0.50)	(0.05–0.59)	(0.32)
Na	0.20–0.73	0.38	0.12–0.38	0.20	0.10–0.61	0.36
	(0.15–0.71)	(0.34)	(0.08–0.28)	(0.15)	(0.07–0.58)	(0.30)
K	0.00–0.04	0.02	0.04–0.07	0.05	0.01–0.05	0.03
	(0.00–0.03)	(0.02)	(0.03–0.06)	(0.04)	(0.01–0.04)	(0.02)
Ca	0.68–0.88	0.76	0.77–0.92	0.82	0.64–0.88	0.73
	(0.59–0.85)	(0.68)	(0.58–0.67)	(0.61)	(0.48–0.75)	(0.62)
Sr	0.04–0.12	0.08	0.07–0.13	0.09	0.04–0.17	0.10
	(0.04–0.09)	(0.07)	(0.05–0.09)	(0.06)	(0.04–0.12)	(0.08)
Mn	0.03–0.04	0.04	0.04–0.05	0.04	0.02–0.08	0.05
	(0.03–0.04)	(0.03)	(0.03–0.04)	(0.03)	(0.02–0.06)	(0.04)
Pb	0.01–0.02	0.01	0.01	0.01	0.01	0.01
	(0.01)	(0.01)	(0.01)	(0.01)	(0.00–0.01)	(0.01)
La	0.01–0.02	0.01	0.01–0.02	0.01	0.01–0.02	0.02
	(0.01)	(0.01)	(0.01)	(0.01)	(0.01–0.02)	(0.02)
Ce	0.00–0.04	0.03	0.03–0.05	0.04	0.03–0.06	0.05
	(0.00–0.04)	(0.03)	(0.02–0.03)	(0.03)	(0.02–0.05)	(0.04)
Pr	0.00–0.01	–	0.00–0.02	0.00	0.00–0.01	–
	(0.00–0.01)	–	(0.00–0.01)	(0.00)	(0.00–0.01)	–
Nd	0.00–0.01	0.01	0.00–0.01	0.01	0.00–0.01	0.01
	(0.00–0.01)	(0.01)	(0.00–0.01)	(0.01)	(0.00–0.01)	(0.01)
U	0.01–0.03	0.02	0.02	0.02	0.02–0.04	0.03
	(0.01–0.03)	(0.02)	(0.01)	(0.01)	(0.02–0.03)	(0.02)
F	0.52–0.89	0.64	0.40–0.67	0.52	0.43–0.74	0.60
	(0.45–0.86)	(0.57)	(0.29–0.49)	(0.39)	(0.30–0.71)	(0.50)
charge	11.98–12.65	12.19	12.00–12.33	12.07	11.99–12.30	12.26
	(11.30–12.47)	(11.75)	(10.84–11.29)	(11.03)	(10.88–12.19)	(11.55)
sum A	1.18–1.77	1.36	1.21–1.49	1.29	1.17–1.47	1.39
	(1.03–1.70)	(1.22)	(0.87–1.09)	(0.96)	(0.84–1.40)	(1.16)

Notes: Fe was assumed as trivalent and Mn as bivalent; atomic proportions were calculated on the basis of Σ(Nb+Ta +Ti +Fe) = 2.00 apfu and Σ(Nb+Ta +Ti +Fe +Si) = 2.00 apfu (values in parentheses), respectively. Sb and Th below detection limits. For analytical precision see text.
* Number of analyses.

Despite the higher resolution of the method, no analysis yielded a pyrochlore completely free of Si. Nevertheless, point analyses of the ultra-thin sample (black filled circles in Fig. 3) fall into two well-separated groups (Table 4). The first one ranges from 0.56 to 2.16 el. wt% Si, whereas the second one ranges from 5.01 to 5.98 el. wt% Si. However, EMPA chemical data that were obtained from a larger excited volume of the sample, show a wider spread in Si content (upward triangles, white and gray circles in Fig. 3).

TEM-EDX data from sample 396c seem to point toward the composition of the "Na-komarovite" (empty square in Fig. 3; data from Balić-Žunić et al. 2002). A reasonable explanation of this feature could be that lamellae of a komarovite-group mineral, whose structure contains pyrochlore-like slabs, are intergrown with pyrochlore. On the other hand, chemical data obtained by EMPA do not support the above interpretation. In fact, the sample 396b shows a radically different trend, pointing straight toward Si, thus suggesting a possible mixture with amorphous silica, in

keeping with the explanation proposed by Voloshin et al. (1989). Samples 396a and 110a do not show any distinct trend.

TEM observations were carried out on areas of different chemical composition. No evidence of crystalline phases other than pyrochlore was obtained. However, Si-poor areas exhibited strong and sharp diffraction peaks, whereas the diffraction pattern from Si-rich areas showed weaker spots with the diffuse diffraction halo typical of the metamict material. Figure 4 includes SAED patterns (along [111] zone axis), bright field (BF) images and EDX spectra obtained from Si-rich and Si-poor areas. It is evident that the most crystalline portions of the pyrochlore structure do not incorporate significant amounts of Si, which is hosted in the portion showing incipient metamictization. Figure 5 shows a high-resolution image with [111] incidence of a more crystalline pyrochlore (corresponding SAED pattern in Fig. 4, upper left). Sharpest dot contrast corresponds to more crystalline areas (darkest portions in the BF image of Fig. 4), whereas metamict areas look aperiodic (bright contrast in Fig. 4). Even at the unit-cell scale, crystalline areas appear homogeneous and free of individual phases or slab intergrowths. Neither crystallization of minerals of the komarovite group nor silica segregations was observed. It seems that Si is enriched in a disordered matrix, which maintains most of the chemical elements originally belonging to the pyrochlore structure. With the increase of radiation damage resulting from alpha decay of Th and U radionuclides minerals become more permeable to fluids so that it can be reasonably assumed that silica-rich fluids have mostly pervaded the metamict areas.

The structural data obtained from X-ray diffraction should result from the prevailing contribution of the portions containing no Si or small amounts of Si together with a minor contribution of the partially metamict Si-rich portions. From the refined atomic coordinates (Table 2), the following bond distances are obtained for crystals 396a and 110a, respectively: A–X (×6) = 2.648(3) and 2.637(4) Å; A–Y (×2) = 2.2560(2) and 2.2460(1) Å (mean <A-O> distance = 2.550 and 2.539 Å); B–X = 1.972(1) and 1.962(1) Å. Due to the possibility of A-site vacancies and the wider range of chemical substitutions at this site, the chemical formula of the pyrochlore group minerals is conventionally normalized to Σ B cations = 2.00. Because the Nb/(Nb + Ta + Ti + Fe) ratio is an almost constant value in each refined crystal (0.88–0.91 and 0.81–0.86 for 396a and 110a, respectively), the mean electron number at the B site obtained on the basis of the chemical data should correspond to that derived from the refinement (Table 2), assuming Si does not enter the B site. The average compositions of the B site for the single crystals (atomic ratios calculated by

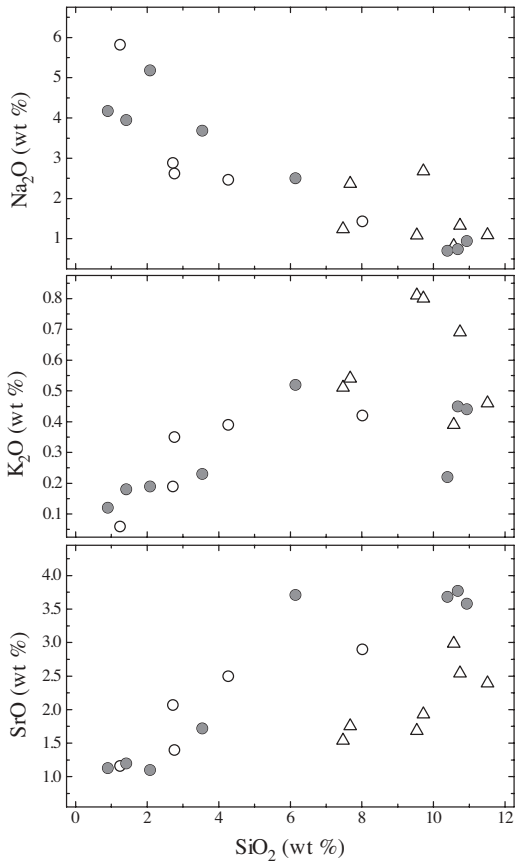

FIGURE 2. Variation of selected chemical components vs. SiO_2 content in pyrochlore from Narssârssuk, (Greenland). White and gray circles refer to 396a and 396b, respectively, triangles refer to 110a.

TABLE 4. Semiquantitative EDX–TEM elemental chemical composition (sample 396c, wt%)

	Si–poor areas		Si–rich areas	
	range	mean (no.* = 5)	range	mean (no.* = 4)
O	19.51–24.78	21.71	22.60–29.76	27.40
F	4.54–8.83	6.45	4.11–9.26	6.87
Na	4.34–6.09	5.18	3.59–4.56	4.29
Si	0.56–2.16	1.18	5.01–5.98	5.59
K	0.00–0.18	0.04	0.59–2.22	1.36
Ca	5.50–6.57	6.06	4.58–5.78	5.27
Ti	1.05–2.55	1.51	1.20–2.04	1.56
Mn	0.00–0.60	0.16	0.33–0.84	0.53
Fe	0.58–1.07	0.84	0.90–1.03	0.99
Sr	0.00–0.96	0.19	2.29–3.42	2.90
Nb	47.70–53.56	51.18	36.63–44.95	39.25
Ce	1.86–2.90	2.51	1.20–2.23	1.68
Pb	0.00–2.54	0.95	0.00–0.84	0.21
U	1.20–2.55	2.05	1.61–2.43	2.09

*Number of analyses.

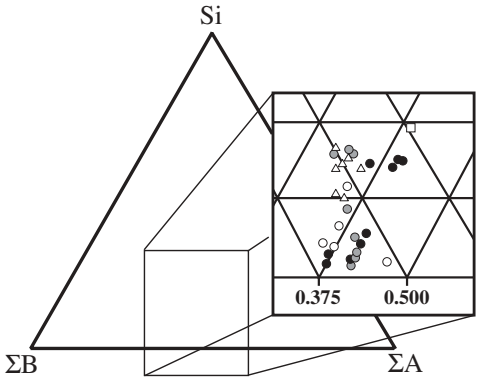

FIGURE 3. Compositional variation (mol%) of pyrochlore from Narssârssuk, (Greenland). Data correspond to the atomic ratios obtained on the basis of Σ(Nb + Ta + Ti + Si + Fe) = 2 apfu (reported in parentheses in Table 3). White, gray, and black circles refer to 396a, 396b, and 396c, respectively, and triangles refer to 110a (this study); square represents "Na-komarovite" (Balić-Žunić et al. 2002).

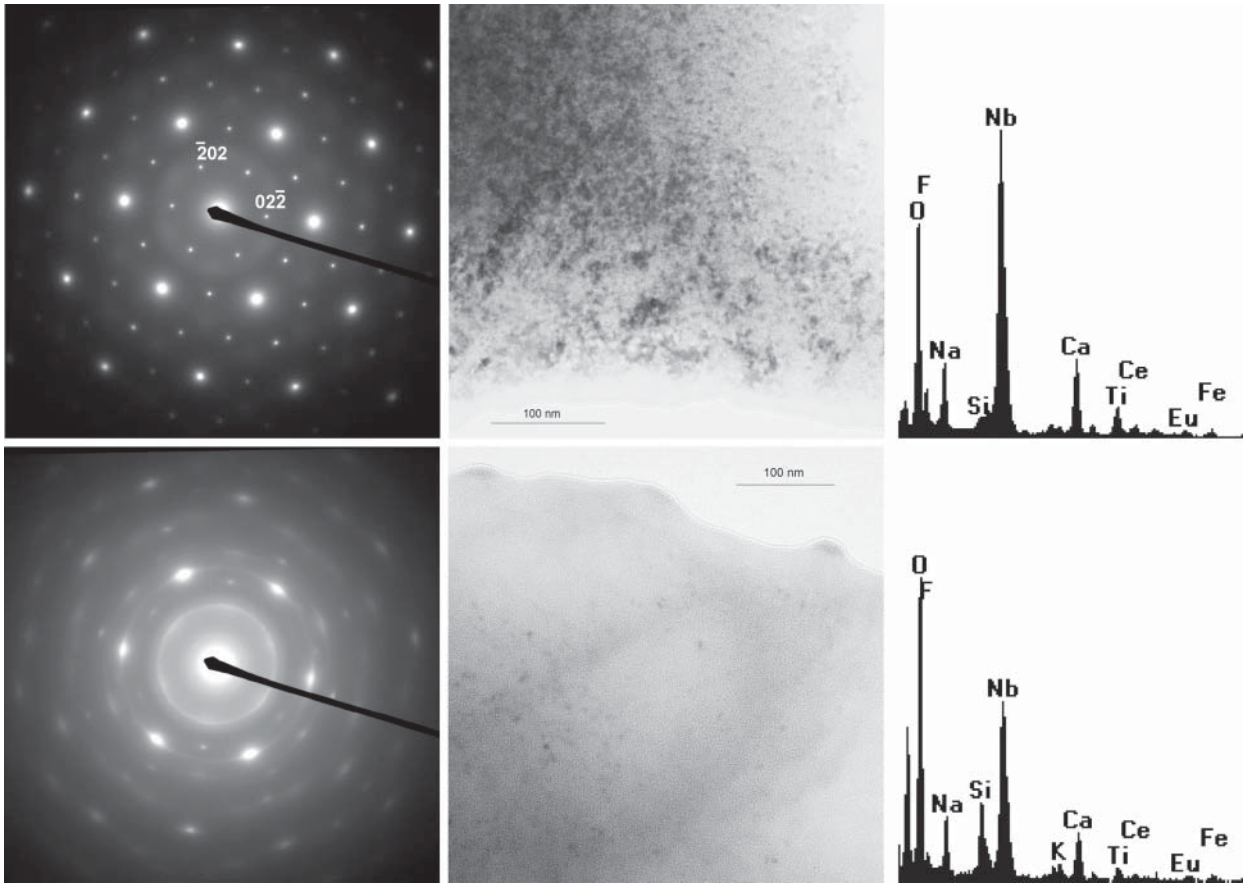

FIGURE 4. From left to right: [111] SAED pattern, BF image, and EDX spectrum obtained from Si-poor (upper) and Si-rich (lower) areas of sample 396c.

excluding Si in Table 3) correspond to a mean electron number of 39.6 (crystal 396a) and 39.4 (crystal 110a), values significantly higher than those obtained by XREF (38.7 and 36.3). To fit the site scattering obtained by XREF, it is sufficient to assign only a fraction of the Si available (0.07 and 0.24 apfu for 396a and 110a, respectively) to the B site. If it were assumed that all Si (0.22 and 0.50 apfu) was incorporated at the B site, site scattering values (36.9 for the crystal 396a and 33.1 for 110a) would be significantly lower than those obtained by XREF. Thus, the following cation populations were tentatively assigned to the B site: B = $[Nb_{1.72}Ta_{0.02}Ti_{0.16}Si_{0.07}Fe_{0.03}]_{\Sigma=2.00}$ (crystal 396a), and B = $[Nb_{1.48}Ta_{0.04}Ti_{0.16}Si_{0.24}Fe_{0.08}]_{\Sigma=2.00}$ (crystal 110a). To test the veracity of this assumption, the observed B-O bond distances and the assumed cation populations were compared for consistency. Due to the complex chemical substitutions and the scarcity of crystal-chemical data in the literature, a comparison among the observed and theoretical bond distances in pyrochlore is not straightforward. Compared to the value of 1.986(1) Å observed in kalipyrochlore with B = 1.80Nb + 0.20Ti (Ercit et al. 1994), the <B-O> distance values in the crystals 396a (1.972 Å) and 110a (1.962 Å) appear low, whereas they are similar to that found in calciobetafite [1.969(3) Å, Mazzi and Munno 1983]. In the latter mineral, however, the B site is occupied by a higher Ti content (B = 0.88 Nb + 0.04 Ta + 1.08 Ti).

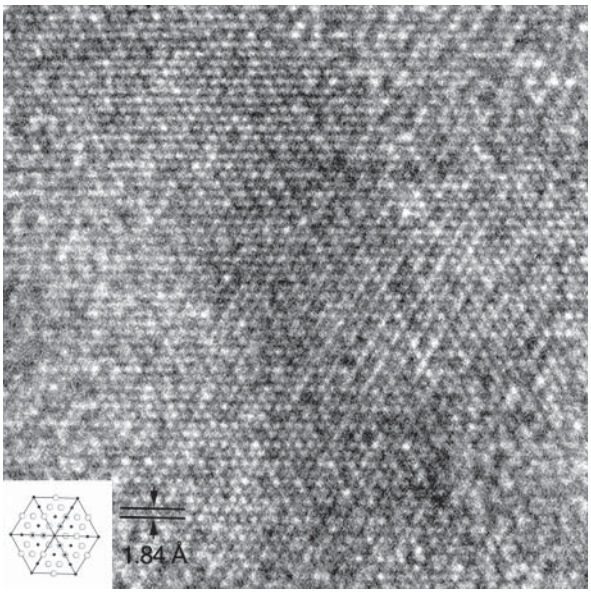

FIGURE 5. HRTEM image obtained along the [111] zone axis and the corresponding structural sketch (lower left) with only A (open circles) and B (filled circles) cations plotted.

$Ti^{4+}$is the smallest cation (ionic radius = 0.605 Å, Shannon 1976) among those normally located on the B site of pyrochlore (Nb^{5+} = 0.64; Ta^{5+} = 0.64; Fe^{3+} = 0.645 Å; Shannon 1976). To model the effect of Ti on the octahedral bond distance, the <B-O> value of synthetic $Y_2Ti_2O_7$ [1.953(2) Å, Becker and Will 1970] and $CaNd(Nb_{1.5}Fe^{3+}_{0.5})O_7$ [1.9909(9) Å, Zhao et al. 2000] were plotted together with data of kalipyrochlore and calciobetafite. The following linear equation was obtained: <B-O> = 1.9902(7) – 0.038(1) [Ti/(Nb + Ta + Ti + Fe^{3+})] (r = –0.999). As shown in Figure 6, the crystals examined exhibit <B-O> values notably lower, in keeping with the hypothesis that significant contents of Si enter the octahedral site. A multiple regression model was therefore conducted to also take into account the effect of Si, using the previous data together with the <B-O> values observed in 396a and 110a and those reported by Reid et al. (1977) for the synthetic $Sc_2Si_2O_7$ [1.761(7) Å] and $In_2Si_2O_7$ [1.800(5) Å] pyrochlore-type compounds: <B-O> = 1.988(7) – 0.21(1)[Si/(Nb + Ta + Ti + Si + Fe^{3+}) – 0.04(1)[Ti/(Nb + Ta + Ti + Fe^{3+})] (r = 0.993). The <B-O> values obtained according to this model on the basis of the B-site population reported above [1.977 Å (396a) and 1.960 Å (110a)] are consistent with the observed values. Thus, assuming Si = 0.07 and 0.24 apfu for 396a and 110a, respectively, the following crystal chemical formulae were obtained on the basis of Σ(Nb + Ta + Ti + Fe) = 1.93 and 1.74:

$$[Na_{0.37}K_{0.02}Ca_{0.73}Sr_{0.07}Mn^{2+}_{0.04}Pb_{0.01}La_{0.01}Ce_{0.03}Nd_{0.01}U^{4+}_{0.02}]_{\Sigma=1.31}[Nb_{1.72}Ta_{0.02}Ti_{0.16}Si_{0.07}Fe_{0.03}]_{\Sigma=2.00}[O_{5.03}(OH)_{0.97}][F_{0.62}(OH)_{0.38}],$$

for crystal 396a, and:

$$[Na_{0.18}K_{0.05}Ca_{0.72}Sr_{0.08}Mn^{2+}_{0.04}Pb_{0.01}La_{0.01}Ce_{0.04}Nd_{0.01}U^{4+}_{0.02}]_{\Sigma=1.16}[Nb_{1.48}Ta_{0.04}Ti_{0.16}Si_{0.24}Fe_{0.08}]_{\Sigma=2.00}[O_{4.63}(OH)_{1.37}][F_{0.46}(OH)_{0.54}],$$

for crystal 110a.

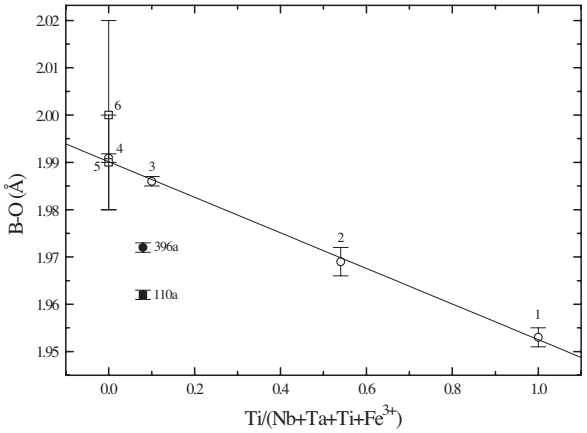

FIGURE 6. Relationship between the octahedral B-O distance and the Ti/(Nb + Ta + Ti + Fe^{3+}) ratio. Filled symbols refer to the single crystals studied. Open symbols (1–6) refer to data from literature: (1) $Y_2Ti_2O_7$ (Becker and Will 1970); (2) calciobetafite (Mazzi and Munno 1983); (3) kalipyrochlore (Ercit et al. 1994); (4) $CaNdNb_{1.5}Fe_{0.5}O_7$ (Zhao et al. 2000); (5) $CaYNb_2O_7$ (Istomin et al. 1997); and (6) $CaNdNb_2O_7$ (Istomin et al. 1997). Due to their high standard deviations (0.01) data for samples 5 and 6 were not included in the regression model.

The corresponding mean electron numbers for the A site are 13.9 and 13.2, which are slightly lower than the values obtained by XREF (14.9 and 13.7, respectively). Nevertheless, the presence of minor amounts of rare earth elements (excluded from the analysis) could account for the small discrepancies observed. The crystals examined are quite similar in chemical composition and structural details, although 110a exhibits a higher Si content coupled with a higher number of A-site vacancies and minor amounts of Na. Both these features contribute to a decrease in total positive charge (12.03 and 11.64 for 396a and 110a, respectively). Uher et al. (1998) suggested that to compensate for the charge deficiency in Si-rich pyrochlores OH^- can substitute for O^{2-} at the X site and/or that molecular H_2O can substitute for (OH^-, F^-) at the Y site. On the basis of the bond valence values calculated using the cation compositions reported above and parameters published by Brown and Altermatt (1985), bond-valence sums of 1.82 and 1.77 v.u. (crystal 396a and 110a, respectively) were obtained at the X site, and bond-valence sums of 0.95 and 0.98 v.u. (crystal 396a and 110a, respectively) at the Y site. These values agree closely with the composition of the anion sites chosen to balance the chemical formulae and rule out the presence of molecular H_2O at the Y site.

The case of thaumasite, the only mineral known to contain Si in six-coordination that is stable at (or near) ambient pressures and temperatures, as well as those of different SiP_2O_7 polymorphs (Bissert and Liebau 1970; Tillmanns et al. 1973; Hesse 1979; Poojary et al. 1994), suggests that the unusual octahedral coordination of Si by O is likely to occur in phases produced at ordinary pressure whenever the only other atoms coordinated to the O atoms are of relatively high electronegativity, such as C, H, or P. According to Edge and Taylor (1971), these relatively electronegative atoms draw electrons from the Si-O bonds, thus lengthening them, decreasing their mutual repulsion, and allowing the increase in Si coordination number to occur. Because bond-valence arguments indicate extensive substitutions of OH^- for O^{2-} on the X site in pyrochlore from Narssârssuk, it is reasonable to hypothesize a local coupling of the Si → (Ti, Nb) substitution with the $OH^- \rightarrow O^{2-}$ substitution leading to an increase of $Si(OH)_6$ groups in the structure upon hydration.

In summary, crystal-chemical considerations combined with TEM-EDX investigations show that a significant fraction (30–50%) of the Si detected by EMPA occupies the octahedral sites of the pyrochlore structure, whereas a larger fraction (50–70%) of Si is concentrated in radiation-damaged portions. However, the present study could not establish the coordination number of Si within the disordered portions, which would require an element-specific technique, such as X-ray absorption spectroscopy. A reduction of coordination number and an increased distortion of B polyhedra, indeed, were found by EXAFS/XANES experiments in fully metamict pyrochlores (Greegor et al. 1985). Note that the "silicified" pyrochlore studied here is not fully metamict. Notwithstanding, heavily damaged domains did not show any trace of other phases, thus leading us to exclude the model of Graham and Thornber (1974), which proposes that pyrochlore decomposes to a microcrystalline arrangement of related structure types. However, our data do not allow us to distinguish between a model involving a short-range crystalline order (Ringwood 1985) and an aperiodic, random network

structure model, similar to that of glass (Ewing 1975; Lumpkin and Ewing 1988).

ACKNOWLEDGMENTS

The authors gratefully acknowledge Ole V. Petersen (Geologisk Museum, Københavns Universitet) for drawing our attention to the problem of "silicified pyrochlores" and for providing the samples. The manuscript was greatly improved by the reviews by A. Chakhmouradian and an anonymous referee. Paul G. Spry (Iowa State University, U.S.A.) is acknowledged for critically reading the manuscript. This work was funded by CNR, Istituto di Geoscienze e Georisorse-sezione di Firenze and by M.I.U.R., P.R.I.N. 2005, project "Complexity in minerals: modulation, modularity, structural disorder."

REFERENCES CITED

Balić-Žunić, T., Petersen, O.V., Bernhardt, H.J., and Micheelsen, H.I. (2002) The crystal structure and mineralogical description of a Na-dominant komarovite from the Ilímaussaq alkaline complex, South Greenland. Neues Jahrbuch für Mineralogie Monatshefte, 2002(11), 497–514.

Bissert, G. and Liebau, F. (1970) Crystal structure of monoclinic silicon phosphate SiP_2O_7 AIII modification: phase with $[SiO_6]$octahedra. Acta Crystallographica, B26, 233–240.

Bøggild, O.B. (1953) The Mineralogy of Greenland. Meddelelser om Grønland, 149(3), 442 p.

Brown, I.D. and Altermatt, D. (1985) Bond-valence parameters obtained from a systematic analysis of the inorganic crystal structure database. Acta Crystallographica, B41, 244–247.

Chakhmouradian, A.R. and Mitchell, R.H. (2002) New data on pyrochlore- and perovskite-group minerals from the Lovozero alkaline complex, Russia. European Journal of Mineralogy, 14, 821–836.

Chakoumakos, B.C. (1984) Systematics of the pyrochlore structure type, ideal $A_2B_2X_6Y$. Journal of Solid State Chemistry, 53, 120–129.

Edge, R.A. and Taylor, H.F. (1971) Crystal Structure of Thaumasite, $[Ca_3Si(OH)_6 \cdot 12H_2O](SO_4)(CO_3)$. Acta Crystallographica, B27, 594–601.

Ercit, T.S., Černý, P., and Hawthorne, F.C. (1993) Cesstibtantiteóa geologic introduction to the inverse pyrochlores. Mineralogy and Petrology, 48, 235–255.

Ercit, T.S., Hawthorne, F.C., and Černý, P. (1994) The structural chemistry of kalipyrochlore, a "hydropyrochlore". Canadian Mineralogist, 32, 417–420.

Ewing, R.C. (1975) The crystal chemistry of complex niobium and tantalum oxides. IV. The metamict state: Discussion. American Mineralogist, 60, 728–733.

Ferraris, G., Makovicky, E., and Merlino, S. (2004) Crystallography of modular materials. IUCr Monographs on Crystallography 15, Oxford University Press. USA.

Finger, L.W. and Hazen, R.M. (1991) Crystal chemistry of six-coordinated silicon: a key to understanding the earth's deep interior. Acta Crystallographica, B47, 561–580.

Flink, G. (1898) Berättelse om en mineralogisk resa i Syd-Grönland sommaren 1897. Meddelelser om Grønland, 14, 221–262.

——— (1901) On the minerals from Narsarsuk on the Firth of Tunugdliarfik in southern Greenland. Meddelelser om Grønland, 24, 7–180.

Graham, J. and Thornber, M.R. (1974) The crystal chemistry of complex niobium and tantalum oxides. IV. The metamict state. American Mineralogist, 59, 1047–1050.

Greegor, R.B., Lytle, F.W., Chakoumakos, B.C., Lumpkin, G.R., and Ewing, R.C. (1985) An investigation of metamict and annealed pyrochlores by X-ray absorption spectroscopy. In C.M. Jantzen, J.A. Stone, and R.C. Ewing, Eds., Scientific Basis for Nuclear Waste Management VIII, p. 655–662. Materials Research Society, Pittsburgh.

Hesse, K.-F. (1979) Refinement of the crystal structure of silicon diphosphate, SiP_2O_7 AIVóA phase with six-coordinated silicon. Acta Crystallographica, B35, 724–725.

Hogarth, D.D. (1977) Classification and nomenclature of the pyrochlore group. American Mineralogist, 55, 1003–1015.

——— (1989) Pyrochlore, apatite and amphibole: distinctive minerals in carbonatite. In K. Bell, Ed., Carbonatites: Genesis and Evolution, p. 105–148. Unwin Hyman Ltd, London.

Hogarth, D.D., Williams, C.T., and Jones, P. (2000) Primary zoning in pyrochlore group minerals from carbonatites. Mineralogical Magazine, 64, 683–697.

Istomin, S.Y., D'yachenko, O.G., Antipov, E.V., and Svensson, G. (1997) Synthesis and characterization of reduced niobates $CaLnNb_2O_7$, *Ln* = Y, Nd with a pyrochlore structure. Materials Research Bulletin, 32, 421–430.

Johan, V. and Johan, Z. (1994) Accessory minerals of the Cínovec (Zinnwald) granite cupola, Czech Republic Part 1: Nb-, Ta-, and Ti-bearing oxides. Mineralogy and Petrology, 51, 323343.

Krivokoneva, G.K., Portnov, A.M., Semenov, E.I., and Dubakina, L.S. (1979) Komaroviteósilicified pyrochlore. Doklady AN SSSR, Earth Science Section, 248, 127130.

Lumpkin, G.R. and Ewing, R.C. (1988) Alpha-decay damage in minerals of the pyrochlore group. Physics and Chemistry of Minerals, 16, 220.

——— (1992) Geochemical alteration of pyrochlore group minerals: Microlite subgroup. American Mineralogist, 77, 179–188.

——— (1995) Geochemical alteration of pyrochlore group minerals: Pyrochlore subgroup. American Mineralogist, 80, 732–743.

——— (1996) Geochemical alteration of pyrochlore group minerals: Betafite subgroup. American Mineralogist, 81, 1237–1248.

Lumpkin, G.R., Foltyn, E.M., and Ewing, R.C. (1986) Thermal recrystallization of alpha-recoil damaged minerals of the pyrochlore structure type. Journal of Nuclear Materials, 139, 113–120.

Mazzi, F. and Munno, R. (1983) Calciobetafite (new mineral of the pyrochlore group) and related minerals from Campi Flegrei, Italy; crystal structures of polymignyte, and zirkelite: comparison with pyrochlore and zirconolite. American Mineralogist, 68, 262–276.

Möller, T., Harjula, R., Pillinger, M., Dyer, A., Newton, J., Tusa, E., Amin, S., Webbe, M., and Araya, A. (2001a) Uptake of ^{85}Sr, ^{134}Cs and ^{57}Co by antimony silicates doped with Ti^{4+}, Nb^{5+}, Mo^{6+} and W^{6+}. Journal of Materials Chemistry, 11, 1526–1532.

Möller, T., Clearfield, A., and Harjula, R. (2001b) The effect of cell dimensions of hydrous mixed metal oxides with a pyrochlore structure on the ion-exchange properties. Chemical Materials, 13, 4767–4772.

Nasraoui, M. and Waerenborgh, J. C. (2001) Fe speciation in weathered pyrochlore-group minerals from the Lueshe and Araxá (Barreiro) carbonatites by ^{57}Fe Mössbauer spectroscopy. Canadian Mineralogist, 39, 1073–1080.

North, A.C.T., Phillips, D.C., and Mathews, F.S. (1968) A semiempirical method of absorption correction. Acta Crystallographica, A24, 351–359.

Poojary, D.M., Borade, R.B., Campbell, F.L., III, and Clearfield, A. (1994) Crystal structure of silicon pyrophosphate (form I) from powder diffraction data. Journal of Solid State Chemistry, 112, 106–112.

Pyatenko, Y.A. (1959) Crystal chemistry and characteristics of minerals of pyrochlore group. Kristallografiya, 4, 204–208 (English abstract).

Reid, A.F., Li, C., and Ringwood, A.E. (1977) High-pressure silicate pyrochlores, $Sc_2Si_2O_7$ and $In_2Si_2O_7$. Journal of Solid State Chemistry, 20, 219–226.

Ringwood, A.E. (1985) Disposal of high-level nuclear wastes: A geological perspective. Mineralogical Magazine, 49, 159–176.

Shannon, R.D. (1976) Revised effective ionic radii and systematic studies of interatomic distances in halides and chalcogenides. Acta Crystallographica, A32, 751–767.

Shannon, R.D. and Sleight, A.W. (1968) Synthesis of new high-pressure pyrochlore phases. Inorganic Chemistry, 7, 1649–1651.

Sheldrick, G.M. (1997) SHELXL97. A program for crystal structure refinement. University of Göttingen, Germany.

Tillmanns, E., Gebert, W., and Baur, W. H. (1973) Computer simulation of crystal structures applied to the solution of the superstructure of cubic silicondiphosphate. Journal of Solid State Chemistry, 7, 69–84.

Uher, P., Černý, P., Chapman, R., Hatr, J., and Miko, O. (1998) Evolution of Nb, Ta-oxide minerals in the Praiv granitic pegmatites, Slovakia. II. External hydrothermal Pb, Sb overprint. Canadian Mineralogist, 36, 535–545.

Voloshin, A.V., Pakhomovskiy, Ya.A., Pushcharovskiy, D.Yu., Nadezhina, T.N., Bakhchisaraitsev, A.Yu., and Kobyashev, Yu.S. (1989) Strontiopyrochlore: composition and structure. Trudy Mineralogicheskogo Muzeya AN SSSR, 36, 12–24 (in Russian).

von Becker, W.J. and Will, G. (1970) Röntgen- und Neutronenbeugungsuntersuchungen an $Y_2Ti_2O_7$. Zeitschrift für Kristallographie, 131, 278–288.

Zhao, X.H., Ruan, S.K., Du, J., Liu, M.L., Jin, M.Z., Li, X.L., Xiong, H., Song, Y.W., and Jia, Y.Q. (2000) Synthesis, crystal structure, Mssbauer spectrum, and magnetic susceptibility of new pyrochlore compound $CaNdFe_{1/2}Nb_{3/2}O_7$. Journal of Solid State Chemistry, 154, 483–487.

MANUSCRIPT RECEIVED JULY 26, 2004
MANUSCRIPT ACCEPTED DECEMBER 25, 2005
MANUSCRIPT HANDLED BY PETER BURNS